Progress In Electromagnetics Research, PIER 104, 221–237, 2010

MULTIFRACTAL DIMENSION AND ITS GEOMETRICAL TERRAIN PROPERTIES FOR CLASSIFICATION OF MULTI-BAND MULTI-POLARIZED SAR IMAGE

H. T. Teng

Faculty of Engineering
Multimedia University
Persiaran Multimedia, Cyberjaya 63100, Malaysia

H. T. Ewe

Faculty of Information and Communication Technology
Universiti Tunku Abdul Rahman
Petaling Jaya, Selangor 46200, Malaysia

S. L. Tan

Faculty of Information and Communication Technology
Department of Mathematical & Actuarial Sciences
Universiti Tunku Abdul Rahman
Petaling Jaya, Selangor 46200, Malaysia

Abstract—Multifractal dimensions D_q for real q are a more general parameter than the fractal dimension in describing geometrical properties. It has been shown that the four multifractal dimensions D_{-1}, D_0, D_1 and D_2 are able to extract different surface information of SAR images. In this paper, we investigate the dimension properties of multifractal dimensions. For land use classification where the textural information on the surface is important, it is necessary to look into the properties of multifractal dimensions with the geometrical properties of terrain. In order to extract the surface information from SAR images, the optimum number of multifractal dimensions to be used in the classification process is considered. To address the suitability of these parameters, these parameters are applied on a multi-band SAR image with regions of different textural information and the results are studied. The abilities of multifractal dimensions in extracting information for different land use

Corresponding author: H. T. Teng (htteng@mmu.edu.my).

classes are considered. In general, although multifractal dimensions provide additional information about the land use classes, there is no clear relation among the land use classes, image polarization and multifractal dimensions.

1. INTRODUCTION

The SAR images of earth terrain have fractal characteristics [1] and fractal dimension has been used as a discriminator in SAR image for different terrain types [2–5]. However, the studies of classification of natural earth terrain using fractal dimension are not conclusive, thus there are more works to be done in improving the method of fractal geometry in this field. The problem arises due to the fact that surfaces with different texture may portray similar fractal dimensions. Evertsz and Mandelbrot [6] suggested that multifractal dimension may be a more appropriate parameter than fractal dimension in describing geometrical properties of a fractal set. They have done a thorough study on multifractal and the study showed that multifractal is a more general parameter than the fractal dimension (or box counting dimension) [7]. Multifractal dimension has also been used as a parameter to segment SAR images [8] and the result is promising. In [9], the multifractal dimensions D_q has shown to provide better surface roughness information in land use classification for SAR image when D_q for $q = -1,\ 0,\ 1,\ 2$ were combined in classifying image, compared to using only a single q value. The fractal dimension D_0 gives the surface roughness information; the entropy dimension D_1 gives the regularity of distribution of points on the surface bounded by its window size; whereas the correlation dimension D_2 gives correlation of points in an area [10]. If D_2 has a higher value for a certain region, it shows that the relationship amongst the points are closely related. The dimension D_{-1} gives the homogeneity of an area. High value of D_{-1} indicates less homogeneous region.

In this paper, the optimum number of multifractal dimensions being used to extract surface information is considered. We showed that surface information as described by D_q for $q > 2$ can be reduced to D_2 and thus it is sufficient to use correlation dimension D_2 to extract surface information since it is more computation expensive to calculate D_q for $q > 2$. Furthermore, we have also shown that fractal properties as described by D_q for $q \leq -1$ are reducible to the case D_{-1}. Hence, the four multifractal dimensions, D_{-1}, D_0, D_1 and D_2 are used to extract different surface information and by combining these information, we are able to characterize the pixel based on more textural information

and thus would help describe the texture image more accurately. These multifractal dimensions were applied to classify a multi-band multi-polarized AIRSAR image with C-, L- and P-bands of HH, HV and VV polarizations with four land use classes. Each band and each polarization gives different spatial information and this information can be further enhanced by calculating their multifractal dimensions D_{-1}, D_0, D_1 and D_2. We compared the effectiveness of multifractal dimensions by applying individual multifractal dimension to classify different land use classes of multi-band multi-polarized image. It is shown that there is no single dimension value that is suitable for all bands and all polarization. The combination of multifractal dimensions portray consistency in classification for all land use classes, while the single multifractal dimension would give different accuracies on these land use classes when applied on images of different bands and polarizations. It is not easy to observe a clear relation between image polarization and multifractal dimensions with different land use classes.

2. MULTIFRACTAL DIMENSIONS

The multifractal dimensions were defined based on partition function. Consider the mass dimension α at the point $\underset{\sim}{x}$, the box $B_\varepsilon(\underset{\sim}{x})$ is a box of radius ε centered at $\underset{\sim}{x}$, $\mu(B_\varepsilon(\underset{\sim}{x}))$ the probability measure or mass in the box. It can be shown that $\mu(B_\varepsilon(\underset{\sim}{x}))$ is proportional to ε^α [10]:

$$\mu\left(B_\varepsilon\left(\underset{\sim}{x}\right)\right) \propto \varepsilon^\alpha. \tag{1}$$

The mass dimension specifies how fast the mass in the box $B_\varepsilon(\underset{\sim}{x})$ decreases as the radius ε approaches to zero [10], in fact,

$$\alpha = \lim_{\varepsilon \to 0} \frac{\log \mu\left(B_\varepsilon\left(\underset{\sim}{x}\right)\right)}{\log \varepsilon}. \tag{2}$$

As an exponent, the exponent α is called the Holder exponent at the point $\underset{\sim}{x}$. If the Holder exponent α does not depend on $\underset{\sim}{x}$, the set is a homogeneous fractal, else it is called an inhomogeneous fractal or a multifractal. For calculation purpose, the coarse Holder exponent $\alpha = \frac{\log \mu(B_\varepsilon(\underset{\sim}{x}))}{\log \varepsilon}$ is used, where the value of α is obtained from the slope of the log-log plot of the graph $\log \mu(B_\varepsilon(\underset{\sim}{x}))$ versus $\log \varepsilon$.

Define a partition function

$$\chi_q(\varepsilon) = \sum_{i=1}^{N} \mu_i^q, \quad q \in R, \tag{3}$$

where μ_i is the measure of the box of size ε and $\sum_{i=1}^{N} \mu_i = 1$, N the number of boxes of size ε that covers the underlying set, and q is a real valued quantity. If μ_i satisfies the multifractal model, the partition function can be related to the Holder exponent by using the power law [6]:

$$\chi_q(\varepsilon) \sim \varepsilon^{\tau(q)}, \tag{4}$$

where $\tau(q) = q\alpha(q) - f(\alpha(q))$ with $f(\alpha)$ being the multifractal spectrum that describes the distribution of the coarse Holder exponent α. Here, the roles played by $\chi_q(\varepsilon)$ and $\tau(q)$ are similar to the roles played by the "partition function" and the "free energy" in thermodynamics. From Equation (4),

$$\tau(q) = \lim_{\varepsilon \to 0} \frac{\log \sum_{i=1}^{N} \mu_i^q}{\log \varepsilon}. \tag{5}$$

The partition function $\tau(q)$ is sometimes written as

$$\tau(q) = (q-1) D_q \tag{6}$$

where D_q is the multifractal dimension. Thus from Equations (5) and (6), D_q can be written as

$$D_q = \frac{\tau(q)}{q-1} = \frac{1}{q-1} \lim_{\varepsilon \to 0} \frac{\log \sum_{i=1}^{N} \mu_i^q}{\log \varepsilon} \tag{7}$$

for $q \neq 1$. For $q = 1$, D_1 is defined by taking the limit when q approaches 1 and by using L'Hopital's Rule:

$$D_1 = \lim_{q \to 1} \frac{1}{q-1} \lim_{\varepsilon \to 0} \frac{\log \sum_{i=1}^{N} \mu_i^q}{\log \varepsilon} = \lim_{\varepsilon \to 0} \lim_{q \to 1} \frac{\sum_{i=1}^{N} \mu_i^q \log \mu_i}{\log \varepsilon \sum_{i=1}^{N} \mu_i^q} = \lim_{\varepsilon \to 0} \frac{\sum_{i=1}^{N} \mu_i \log \mu_i}{\log \varepsilon} \tag{8}$$

since the term $\sum_{i=1}^{N} \mu_i^q$ in the denominator approaches to $\sum_{i=1}^{N} \mu_i$ as $q \to 1$, and $\sum_{i=1}^{N} \mu_i = 1$. This dimension corresponds to the information dimension or entropy dimension. It gives the average information contained in a system. For measuring surface information, higher value of D_1 can be interpreted as a measure for surface with more uniform distributed intensity values, whereas lower D_1 gives information of a

surface with non-uniform distribution intensity values in a particular region. The surface roughness information can be obtained indirectly, and D_1 gives the randomness of points in a region, with the degree of randomness decreases as D_1 increases.

For $q = 0$, $D_0 = -\lim_{\varepsilon \to 0} \frac{\log N}{\log \varepsilon}$ and it corresponds to the conventional fractal dimension which gives the information on surface roughness.

For cases where $q \geq 2$ and $q < -1$, the interpretation is given in the following subsections. For the first time, we will associate geometrical description with D_q for $q \leq -1$. We will also show that it is sufficient to consider D_{-1} for describing fractal properties as fractal properties described by D_q for $q \leq -1$ are reducible to the case D_{-1}.

2.1. Multifractal Dimension D_q, $q \geq 2$

Based on the alternative approach shown in [10], we will show that fractal properties as described by D_q for $q \geq 2$ are reducible to the case D_2. For $q \geq 2$, Peitgen et al. [10] considered that

$$D_q = \frac{1}{1-q} \lim_{\varepsilon \to 0} \frac{\log \sum_{k=1}^{N} p_k^q}{\log \frac{1}{\varepsilon}} \tag{9}$$

where $p_k = \mu(B_k)$, the natural measure of the disk B_k (viz., the percentage of points visiting the orbit in the box B_k). Since $\sum_{k=1}^{N} p_k^q \propto C_q(\varepsilon)$, with $C_q(\varepsilon)$ gives the probability that q-tuples $(x_{i1}, x_{i2}, \ldots, x_{iq})$, $i = 1, 2, \ldots, m$, of different points from the orbit satisfying the Euclidean distance $d(x_{il}, x_{ir}) < \varepsilon$ for $l, r = 1, 2, \ldots, q$, thus

$$D_q = \frac{1}{1-q} \lim_{\varepsilon \to 0} \frac{\log C_q(\varepsilon)}{\log \frac{1}{\varepsilon}} \tag{10}$$

since $\sum_{k=1}^{N} p_k^q = kC_q(\varepsilon)$ for some constant k, and the value of $\frac{\log k}{\log \frac{1}{\varepsilon}} \to 0$ as $\varepsilon \to 0$.

Using this approach, for $q = 2$,

$$D_2 = -\lim_{\varepsilon \to 0} \frac{\log C_2(\varepsilon)}{\log \frac{1}{\varepsilon}} \tag{11}$$

with $C_2(\varepsilon)$ measures the correlation between pairs of points satisfying $d(x_{i1}, x_{i2}) < \varepsilon$. Thus D_2 is called the correlation dimension. For small fixed ε, behavior of D_2 is similar to the behavior of $C_2(\varepsilon)$. For rougher surface, $C_2(\varepsilon)$ has low value as the number of 2-tuples with

the distances between points (pixels) less than ε are low, hence D_2 would be low. Whereas for smoother surface (or homogeneous region), the correlation $C_2(\varepsilon)$ is higher and hence D_2 would have higher value.

Clearly, the number of 3-tuples (x_{i1}, x_{i2}, x_{i3}) satisfying $d(x_{il}, x_{ir}) < \varepsilon$, $l, r = 1, 2, 3$ is less than the number of 2-tuples (x_{i1}, x_{i2}) satisfying $d(x_{i1}, x_{i2}) < \varepsilon$, then $C_3(\varepsilon) \leq C_2(\varepsilon)$ and hence $D_3 \leq D_2$, which coincides with the property that D_q is a non-increasing function.

Consider an image and let's take a look at a window of size $L \times L$. We calculate the value of D_3 for each window. If a window has high D_3 value, we conclude that the value of $C_3(\varepsilon)$ is also high as they are related by Equation (10). High value of $C_3(\varepsilon)$ means the relationship between any two points of 3-tuples has high probability to have similar intensity and thus we may conclude that the window covers homogeneous region. Conversely, low value of D_3 would mean that the region covered is less homogeneous.

The property of D_q for all $q > 3$ can be generated from the above based on similar argument. Note that we have a non-increasing function D_q as q increases [10]. This is confirmed as D_q and $C_q(\varepsilon)$ have similar behavior, and $C_q(\varepsilon)$ decreases as the number of q-tuples $(x_{i1}, x_{i2}, \ldots, x_{iq})$ satisfying $d(x_{il}, x_{ir}) < \varepsilon$, $l, r = 1, 2, \ldots, q$, $i = 1, 2, \ldots, m$, decreases as q increases. Also, q-tuples for $q \geq 3$ can be decomposed into more 3-tuples. Thus, higher value of D_3 would certainly lead to high values of other D_q's for $q > 3$, and vice versa. Hence, due to expensive computation, evaluation on D_q for $q > 3$ is not necessary, and we choose only D_{-1}, D_0, D_1 and D_2 for the study in this paper.

Though there is no direct information given by D_q on surface roughness, but from the correlation of points (pixels of image) in the window, the surface information can be deduced indirectly. For rough surface, there are more neighbourhood points of different intensity and hence the number of points with $d(x_{il}, x_{ir}) < \varepsilon$ decreases and thus implies low D_q. For homogeneous surface, there are more neighbourhood points of similar intensity and hence the points satisfying $d(x_{il}, x_{ir}) < \varepsilon$ are more, thus gives high D_q.

2.2. Multifractal Dimension D_q, $q \leq -1$

For D_q with finite $q \leq -1$, the multifractral fractal dimension is

$$D_q = \frac{1}{q-1} \lim_{\varepsilon \to 0} \frac{\log \sum_{i=1}^{N} \mu_i^q(\varepsilon)}{\log \varepsilon} = \frac{1}{-k-1} \lim_{\varepsilon \to 0} \frac{\log \sum_{i=1}^{N} \frac{1}{\mu_i^k(\varepsilon)}}{\log \varepsilon} \quad \text{for} \quad q = -k,\ k > 0. \tag{12}$$

Let $m(k) = \sum_{i=1}^{N} \frac{1}{\mu_i^k(\varepsilon)}$, $k > 0$. Consider $\mu_i^k(\varepsilon)$ as the number of points such that $|r_i - x| < k\varepsilon^k$ for all $x \in B_i(\varepsilon)$ over total points in an open ball $B_i(\varepsilon)$ centered at r_i. In other words, $\mu_i^k(\varepsilon)$ gives the probability that the number of points x satisfying $|r_i - x| < k\varepsilon^k$ that exist in $B_i(\varepsilon)$, and $\sum_i \mu_i = 1$. As k increases, $\mu_i^k(\varepsilon)$ decreases for fixed small ε, since the possible regions such that the inequality being satisfied is reduced. As a result, its inverse $\frac{1}{\mu_i^k(\varepsilon)}$ is able to capture regions with scattered points such that $|r_i - x| < k\varepsilon^k$ for all $x \in B_i(\varepsilon)$. If its value is high, the region has very few points satisfying the inequality over the region. If the value is low, the region is filled with more points satisfying the inequality. The term $m(k) = \sum_{i=1}^{N} \frac{1}{\mu_i^k(\varepsilon)}$ measures the total dispersion of points in the whole region with respect to ε-measurement, satisfying $|r_i - x| < k\varepsilon^k$ in all disjoint $B_i(\varepsilon)$'s. Geometrically, the value $m(k)$ describes the non-homogeneity of a region, with bigger value represents a less homogeneous region.

Since $0 \leq \mu_i(\varepsilon) \leq 1$, we have $0 < \mu_i^k(\varepsilon) \leq \mu_i(\varepsilon) \leq 1$ and $1 \leq \frac{1}{\mu_i(\varepsilon)} \leq \frac{1}{\mu_i^k(\varepsilon)} < \infty$ for $k > 0$. When $\mu_i(\varepsilon) \to 0$, then $\frac{1}{\mu_i(\varepsilon)} \to \infty$. For fixed k and $\varepsilon > 0$, if $\mu_i^k(\varepsilon) \sim 1$, then $\frac{1}{\mu_i^k(\varepsilon)} \sim 1$, and the points are mostly concentrated at the center of $B_i(\varepsilon)$ as k increases.

It is obvious that the number of points satisfying the condition $|r_i - x| < k\varepsilon^k$ gets lesser as $k \to \infty$. Those points satisfying $|r_i - x| < k\varepsilon^k$ when k is large obviously also satisfy $|r_i - x| < k\varepsilon^k$ when k is small, for points in the same $B_i(\varepsilon)$ for some i and some ε. Hence it is sufficient to just consider small k, in particular when $k = 1$.

2.3. Multifractal Dimensions and Geometrical Surface Information

We notice that all multifractal dimensions display localized properties. This can be viewed from their graphs with respect to total measure in a certain region. For each region covered by a window, the multifractal dimensions in each window containing intensity values in various combinations will show an arc, with the biggest arc being displayed by the dimension values in the window containing the absolute maximum intensity. For example, consider a region having intensity values from 1 to 5. Figure 1 shows the relation of multifractal dimension D_{-1} with its total measure for $\varepsilon = \frac{1}{3}$, i.e., for window size 3×3. If the maximum intensity in a local region of size 3×3 is 4, the graph of multifractal

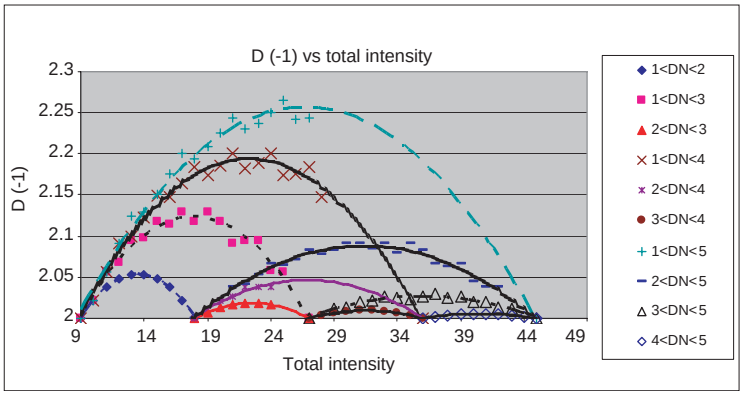

Figure 1. Local properties of multifractal dimension D_{-1} versus total intensity value in a local region. 'DN' refers to intensity values in the local region.

dimension D_{-1} is as shown by the brown color arc. For a local region 3×3 that contains absolute maximum intensity 5, the dimension values for D_{-1} are displayed by the dull green color arc, which is the biggest arc. This localized property is true for all multifractal dimensions.

For homogenous regions of either low or high intensity values only, the dimension values lie at both ends of the arc. When the region is non-homogenous, the values are grouped in the middle of arc, and hence give higher dimension values.

For $q = 1$ which is the entropy dimension, it is a limiting case where the dimension values of other D_q's, $q > 0$, converge to D_1 when $q \to 1$. We generated the graph for a small region of size 3×3 with intensity values vary from 1 to 3, for D_1, D_2, $D_{0.5}$ and $D_{1.5}$. The graph generated, as shown in Figure 2, has localized property coincides with the results for computing D_1 from the multifractal dimension D_q. It is noted from the figure that as q increases to 1 and as q decreases to 1, the dimension values approach to D_1. This shows that D_1 is a limiting case.

For fractal properties description, it is sufficient to use four multifractal dimensions which are linearly independent cases: D_{-1}, D_0, D_1, D_2. Note that for $q < -1$, the cases are reducible to D_{-1} as cases that satisfy these D_q's are all satisfying D_{-1}. For $q \geq 2$, all higher cases can be reduced to D_2. The four multifractal dimensions D_{-1}, D_0, D_1, D_2 cover all the spatial information required, and if necessary, we may replace D_{-1} by using a more negative q value in order to extract surface information of small intensity values. Similarly, D_2 can be replaced by using a more positive q if required.

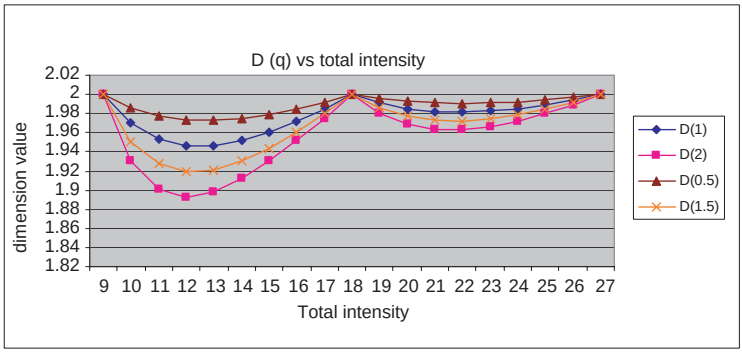

Figure 2. Graph showing D_1 as the limiting case for D_q's, $q > 0$, for sub-regions of size 3×3 from a region having intensity values varying from 1 to 3.

However, since D_q's are related in certain degree, the surface properties cannot be decomposed into individual D_q's, $q = -1$, 0, 1, 2. In other words, D_q's have some geometrical properties in common. As such, it is expected that for surface with vast different characteristics, multifractal dimensions would be able to give more significant results compared with the surface of similar features.

Based on the findings above, we use multifractal dimensions to classify a multi-band multi-polarized AIRSAR image with four land use classes. The characteristics and information extracted by multifractal dimensions and their relation with multi-band multi-polarized images are studied. From the classification results, we compared the effectiveness of multifractal dimensions in classifying multi-band multi-polarized image based on individual multifractal dimensions as well as each band and each polarization for different land use classes.

3. LAND USE CLASSIFICATION OF MULTI-BAND MULTI-POLARIZED IMAGE

The multifractal dimensions are used as parameters in classifying four land use classes for an appropriately subset region of an AIRSAR image of Muda Merbok area, Kedah. This image is not easy to classify as areas of different land use are mixed together. The AIRSAR image for the study area was taken on 19 September 2000 with the geographical coordinates of 5.6022°N.–6.3892°N. Lat. and 100.3867°E.–100.5034°E. Long., with 2540 samples and 13094 lines. There are three bands with three polarizations, hence 9 images are given: *C-HH*, *C-VV*,

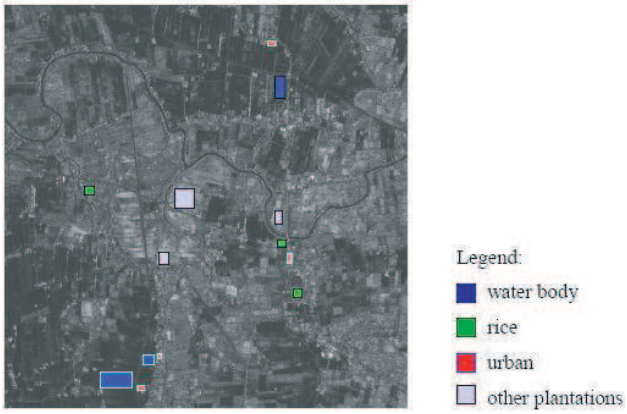

Figure 3. Training areas for *C-HH* image which were selected after a field trip to the areas. The training areas are the same for images of all other bands and polarizations.

C-HV, *L-HH*, *L-VV*, *L-HV*, *P-HH*, *P-VV*, *P-HV*. Its resolution is 5 meters. The *P*-band images are very noisy especially at the regions nearer to urban areas (e.g., Alor Setar, Sungai Petani and Gurun) due to radio frequency interference. These 9 images were filtered using Lee filter for speckle reduction. The preprocessing was done on the images of all bands and all polarizations where the operation of slant-range to ground-range conversion was done and the pixel dimension was adjusted to 5 m × 5 m. Figure 3 shows the selected region of size 1024 × 1024 pixels and the training areas.

In order to apply multifractal dimensions on SAR images, a virtual 3-dimensional surface was first constructed and then covering method [3] was used to calculate multifractal dimensions. The four multifractal dimensions where $q = -1,\ 0,\ 1$ and 2, were calculated for all pixels in each training area and in all nine multi-band multi-polarized images. Averages of each multifractal dimension at each training area were then calculated. A windowing technique was applied with odd window sizes chosen and the calculated multifractal dimensions values were assigned to the central pixel of each window. A vector of four components $(D_{-1},\ D_0,\ D_1,\ D_2)$ was assigned to each pixel. Minimum Euclidean distance classifier was applied to do the classification for these data and a comparison of classification results was done. The processing was done using nine images, initially for individual image and later using a "VOTING" process with equal weight for all nine images. The "VOTING" process is defined as follows. For each individual image, each pixel has been assigned a land

use class under the classification using minimum Euclidean distance classifier, which may be different from one image to another image of different band and different polarization. Under this "VOTING" process, we consider the pixel $(i,\ j)$ in the nine images, and the number of times that a land use class is assigned to this pixel is noted. For a pixel that has been classified most times for this particular land use class, the pixel will be "voted" to be of this land use class. Later, the "VOTING" process was performed with the P-band images being singled out because of its noise at the southern region of the selected area, which may be due to the radio frequency interference as the telecommunication activity was very active at this region. The two sets of resulted images using voting process were compared. Accuracy assessment was done for the two sets of results.

The classification was done using 3×3, 5×5, 7×7 and 9×9 window sizes. We found that when the window size was smaller than 7×7, there was too little information captured whereas for larger window size, some of the information were lost due to averaging of information. After the analysis, window size 7×7 was found to be optimum. As we intended to investigate the abilities of multifractal dimensions in classifying different land use classes, the accuracy assessment was done on these training areas and thus the accuracy was expected to be high. The summary is as shown in Table 1.

Table 1. Summary of accuracy assessment for classified images where each pixel has been assigned the vector-form of four multifractal dimension values using window size 7×7. "VOTING" is referred to the voting process using equal weight for 9 images.

Producer's accuracy

	Water body	Rice	Other Plantation	Urban	Overall accuracy
CHH	70.48	93.29	83.83	88.07	77.52
CHV	70.11	60.57	73.50	88.99	71.05
CVV	60.97	88.21	60.23	84.40	62.95
LHH	80.07	39.63	90.29	75.23	81.13
LHV	87.23	56.50	86.95	100.00	85.17
LVV	76.76	50.81	77.13	68.81	74.96
PHH	61.54	38.21	60.70	92.66	60.07
PHV	12.77	35.37	58.61	93.58	33.36
PVV	60.19	26.02	78.96	100.00	65.69
VOTING	86.70	83.94	97.29	97.25	90.77

Table 2. Accuracy assessment for classified images using C- and L-band images where each pixel has been assigned the vector-formed of four multifractal dimensions values using window size 7×7. "VOTING-6" was referred to the voting process using equal weightage applied on six polarized images of C- and L-bands.

Producer's accuracy

	Water body	Rice	Other Plantation	Urban	Overall accuracy
VOTING-6	88.58	95.53	91.46	91.74	90.23

Overall, the classified image by voting process gives above average results for all classes. Its overall accuracy is 90.77%, which is the highest amongst other classification over other single polarized images. However, for individual classes, L-HV gives the best accuracy for "water body", C-HH gives 93.29% of accuracy for "rice", "VOTING" gives accuracy of 97.29% for "other plantations", whereas L-HV and P-VV classifies "urban" with accuracy of 100%.

From Table 1, it is also observed that L-band image of any polarization is most suitable to be used for classification of "water body" and "other plantations" whereas C-HH image is best used to classify "rice". P-band images are generally good for classification of "urban" areas but not suitable for classification of land use classes "water body" and "rice". It gives very low accuracy in the classification of these land use classes and thus results to low overall accuracy by using P-band. This is further confirmed in the accuracy assessment when P-band has been singled out from the analysis by using a voting process, as shown in Table 2. In this analysis involving only C- and L-band images, the direct implication is that the accuracy for both "water body" and "rice" has increased from 86.70% to 88.58% and 83.94% to 95.53% respectively, whereas the accuracy for "other plantations" has dropped from 97.29% to 91.46% and urban area has dropped from 97.25% to 91.74%. On the whole, classification using all bands and all polarized images has overall accuracy of 90.77%, which performs slightly better than using only C- and L-band images that has overall accuracy of 90.23%. Hence, the P-band images may be excluded in the land use classification by using the vector-form multifractal dimensions. The classified images into four land use classes using vector-form multifractal dimensions are shown in Figure 4.

Investigation has also been carried out to investigate the effect of each multifractal dimension on different band of images in the classification. Table 3 shows a summary on the accuracy assessment for the classified images. The accuracy values displayed are the highest value obtained among the combinations of multifractal dimension and polarization used.

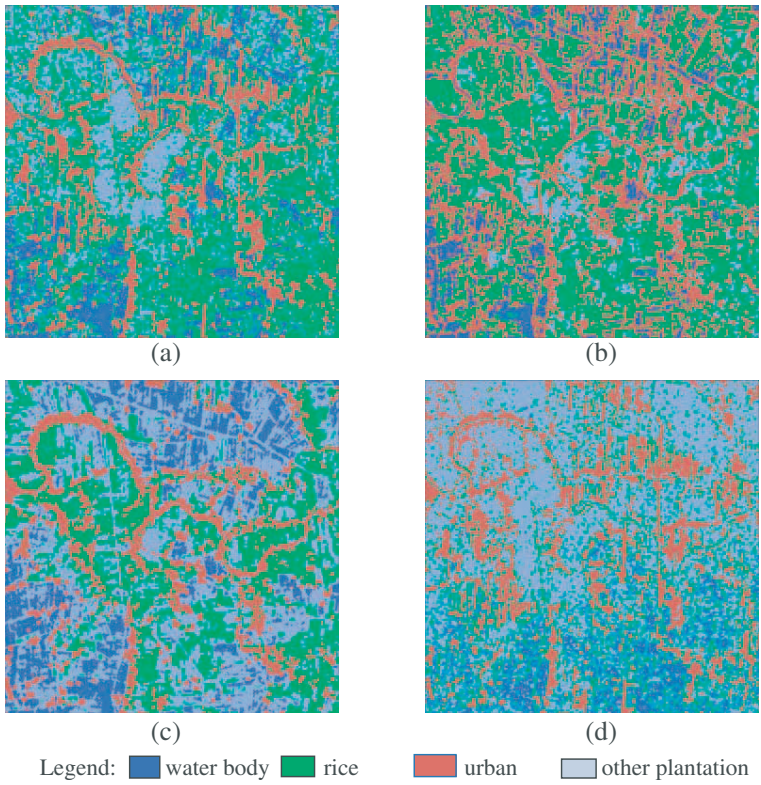

Figure 4. Classified images for multi-band, multi-polarised AIRSAR images of selected Muda Merbok area, Kedah, using window size 7×7. (a) Classified image using equal weightage for nine polarized images, having highest overall accuracy and highest accuracy for "other plantations". (b) Classified image of *C-HH* having highest accuracy for "rice". (c) Classified image of *L-HV* having highest accuracy for "water body" and "urban". (d) Classified image of *P-VV* having highest accuracy for "urban".

Table 3. Summary of accuracy assessment for classified images using one multifractal dimension on images of different polarizations.

Land use class	Accuracy (band/dimension used)
Water body	100% (C-HV/D_0)
Rice	92.07% (C-HH/D_0)
Other plantations	84.46% (L-HH/D_{-1})
Urban	100% (L-HV/D_0)
Overall accuracy	88.28% (L-HV/D_0)

From Tables 1 and 3, it is obvious that classification using vector-form multifractal dimension under a voting process generally gives better accuracies compared to using a single multifractal dimension over single polarized images. For a single multifractal dimension when combined with a specific polarized image, it classifies certain classes well. For example, the class "water body" is best classified using fractal dimension D_0 on C-HV image and the class "other plantation" is best classified using D_{-1} on L-HH image. In general, D_0 classifies C-band "water body" and "rice" better; it also classifies L-band "urban" better whereas D_{-1} classifies L-band "other plantation" better. The

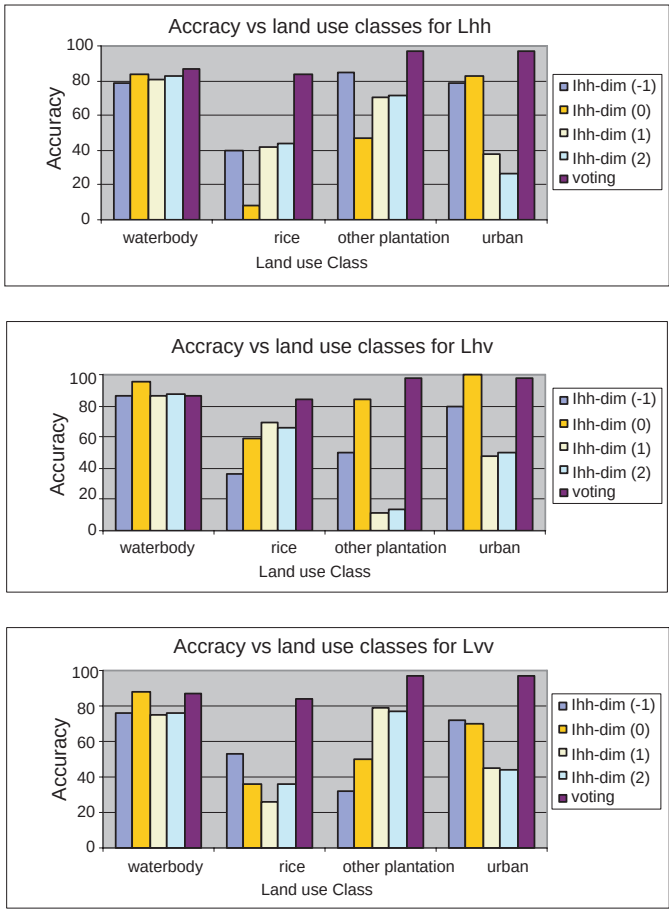

Figure 5. Figure showing relations of L-band multi-polarized images with multifractal dimensions and land use classes.

result corresponds to the relationship between the wavelengths and the targeted objects, where C-band is normally responded better to upper surfaces information (e.g., water surface and rice) and L-band for intermediate surfaces (e.g., tree trunks and buildings). From our results, it is also shown that the usage of P-band images in the classification of this region is very limited as it gives very poor accuracy for most of the classes and thus can be ignored. This may be due to the reason that the selected region is nearer to the town and has more radiofrequency interference.

Figure 5 shows the relation of L-band with multifractal dimensions and land use classes. From the figure, classification using vector-form multifractal dimensions under a voting process generally gives better accuracies amongst all other single multifractal dimension for the classification of "rice", "other plantations" and "urban". It gives moderately good accuracies for classification of "water body", which is about 87%. In general, it portrays consistency in classification for all land use classes, while the single multifractal dimensions would give different accuracies when applied using different bands and polarizations.

Table 4. A summary for multifractal dimensions.

$q = -1$	$D_{-1} = \frac{1}{-2}\lim_{\varepsilon \to 0} \frac{\log \sum_{i=1}^{N} \frac{1}{\mu_i}}{\log \varepsilon}$	Homogeneity dimension	• Measures homogeneity of a region • For homogeneous region, D_{-1} value is low • For non-homogeneous region, D_{-1} value is high
$q = 0$	$D_0 = -\lim_{\varepsilon \to 0} \frac{\log N}{\log \varepsilon}$	Fractal dimension	• Gives surface roughness information • Rougher surface has higher D_0 value
$q = 1$	$D_1 = \lim_{\varepsilon \to 0} \frac{\sum_{i=1}^{N} \mu_i \log \mu_i}{\log \varepsilon}$	Entropy dimension	• Region with more uniform values has higher D_1 value
$q = 2$	$D_2 = \lim_{\varepsilon \to 0} \frac{\log \sum_{i=1}^{N} \mu_i^2}{\log \varepsilon}$	Correlation dimension	• Measures correlation between pairs of points • Regular regions have higher D_2 value

4. CONCLUSION

Table 4 summarizes the surface information being extracted using four multifractal dimensions, D_{-1}, D_0, D_1 and D_2.

Multifractal dimensions, when combined in a vector form, are able to describe more surface information than a single multifractal dimension. In this paper, we have associated geometrical properties to negative dimension. We have shown that surface information as described by D_q for $q > 2$ can be reduced to D_2 and thus it is sufficient to use correlation dimension D_2 to extract surface information since it is more computation expensive to calculate D_q for $q > 2$. Further more, we have also shown that fractal properties as described by D_q for $q \leq -1$ are reducible to the case D_{-1}. Hence, the four multifractal dimensions, D_{-1}, D_0, D_1 and D_2 are able to extract different surface information and by combining these information, we are able to characterize the pixel based on more textural information. However, multifractal dimensions are related in certain degree; thus the surface properties cannot be decomposed into each D_{-1}, D_0, D_1 and D_2. Thus the representation by these four multifractal dimensions has overlapped properties.

Multifractal dimensions are used as a suitable set of parameters to extract the information from the multi-band multi-polarized AIRSAR images for land use classification. In general, a clear relation among land use classes, image polarization and multifractal dimensions is not easy to observe. The classification of specific land use classes using a specific polarization and a specific multifractal dimension may not be optimal. There is no single dimension value that is suitable for all bands and all polarization. In fact, it is found that except for classification of "water body" using L-band associated with any multifractal dimensions, other classes are better classified using the combination of all four multifractal dimensions in a vector-form. It is further noticed that the vector-form multifractal dimensions is not suitable for land use classes of similar terrain information due to its limitation in giving a perfect decomposition of surface properties. Further studies in future in this will help improve our understanding in utilizing suitable combination of multifractal dimensions in land use classification.

REFERENCES

1. Pentland, A. P., "Fractal-based description of natural scenes," *IEEE Transactions on Pattern Analysis and Machine Intelligence*, Vol. 6, No. 6, 661–674, 1984.

2. Chan, K. L., "Fractal based texture analysis," *Singapore ICCS/ISITA'92*, Vol. 1, 102–106, 1992.
3. Ewe, H. T., W. C. Au, R. T. Shin, and J. A. Kong, "Classification of SAR images using a fractal approach," *PIERS Proceedings*, 493, Los Angeles, USA, 1993.
4. Keller, J. M., S. Chen, and R. M. Crownover, "Texture description and segmentation through fractal geometry," *Computer Vision, Graphics, and Image Processing*, Vol. 45, 50–166, 1989.
5. Marazzi, A., P. Gamba, A. Mecocci, and E. Costamagna, "A mixed fractal/wavelet based approach for characterization of textured remote sensing images," *IEEE International Geoscience and Remote Sensing Symposium Proceedings, IGARSS'97*, Vol. 2, 655–657, 1997.
6. Evertsz, C. J. G. and B. B. Mandelbrot, "Multifractal measures," *Chaos and Fractals: New Frontiers of Science*, H.-O. Peitgen, H. Jurgens, and D. Saupe (eds.), 849–881, Springer Verlag, New York, 1992.
7. Falconer, K., *Fractal Geometry*, John Wiley, 1990.
8. Yeo, T. S. and G. Du, "A multifractal approach for auto-segmentation of SAR images," *IEEE Geoscience and Remote Sensing Symposium Proceedings, IGARSS 2001*, Vol. 5, 2301–2303, 2001.
9. Teng, H. T., H. T. Ewe, and S. L. Tan, "A multifractal approach for classification of SAR image," *Proceedings Third National Microwave Remote Sensing Seminar*, MACRES, Kuala Lumpur, Sep. 28, 2004.
10. Peitgen, H.-O., H. Jurgens, and D. Saupe, *Chaos and Fractals — New Frontiers of Science*, Springer-Verlag, New York, 1992.